PROCEEDINGS OF SPIE

SPIEDigitalLibrary.org/conference-proceedings-of-spie

Enhancing the accuracy of solar polarimetry by coalescing slow and fast modulation: method description and first performance tests

Franziska Zeuner, Daniel Gisler, Michele Bianda, Renzo Ramelli, Svetlana Berdyugina

Franziska Zeuner, Daniel Gisler, Michele Bianda, Renzo Ramelli, Svetlana V. Berdyugina, "Enhancing the accuracy of solar polarimetry by coalescing slow and fast modulation: method description and first performance tests," Proc. SPIE 12184, Ground-based and Airborne Instrumentation for Astronomy IX, 121840T (29 August 2022); doi: 10.1117/12.2629250

SPIE.

Event: SPIE Astronomical Telescopes + Instrumentation, 2022, Montréal, Québec, Canada

Enhancing the accuracy of solar polarimetry by coalescing slow and fast modulation: method description and first performance tests

Franziska Zeuner[a], Daniel Gisler[a,b], Michele Bianda[a,c], Renzo Ramelli[a], and Svetlana V. Berdyugina[a,b,c]

[a]IRSOL Istituto Ricerche Solari "Aldo e Cele Daccò", Università della Svizzera italiana, CH-6605 Locarno, Switzerland
[b]Leibniz-Institut für Sonnenphysik (KIS), D-79104 Freiburg, Germany
[c]Euler Institute, Università della Svizzera italiana (USI), CH-6900 Lugano, Switzerland

ABSTRACT

The polarimetric zero-level accuracy of spectropolarimetric measurements with ground-based solar telescopes usually suffers from systematic telescopic and instrumental effects which are difficult to model, and therefore, cannot be easily removed during post-measurement data reduction. Here, a novel measurement method to enhance the zero-level accuracy to an unprecedented level of such compromised measurements is presented. The method is comprised of adding a slow polarization modulation (<1 Hz) before any polarizing component of the telescope to a high-sensitivity polarimeter with fast modulation (>1 kHz). This additional slow modulation significantly mitigates systematic instrumental polarization signals induced by the telescope and post-focus instruments such as polarimetric offsets or cross-talk between polarization states. We present the results and limitations learned from implementing the method at the 45 cm Gregory-Coudé telescope at IRSOL, Locarno. The slow modulation is performed with a low-cost zero-order retarder film mounted in front of the telescope and is combined with the fast modulating Zürich IMaging POLarimeter (ZIMPOL). We find that the ground zero of polarization normalized to the intensity is determined within a few 10^{-5}. This level is consistently achieved over a wide wavelength range in the visible. An improvement of up to a few orders of magnitude for cases where the polarization offset induced by the telescope is as high as 10^{-2} is achieved. This measurement technique allows for enhancing the zero-level accuracy of solar polarimetry, which is crucial for scattering polarization measurements and their theoretical interpretations.

Keywords: polarimetry, solar telescopes

1. INTRODUCTION

Polarimetry and spectropolarimetry are of paramount importance to study the Sun in near-ultraviolet, visible and near-infrared light, through which magnetic fields and other physical aspects in multiple layers of the solar atmosphere are investigated. Besides high spectral (<100 mÅ), spatial (<1 arcsec) and temporal (<30 s) resolution, observations require high polarimetric sensitivity (on the order of $<10^{-4}$ in fraction of the intensity) in order to allow studying the most elusive and controversial regimes of solar magnetism.[1,2] Polarimetric sensitivity, as a measure for the detectable polarization amplitude with respect to a (noisy) background, is coupled to the precision and amplitude accuracy of the measurement system. Considering that the background in spectropolarimetric measurements is usually the continuum polarization between spectral lines, the overwhelming majority of the observed polarization signals in the solar spectrum are measurements relative to the continuum. For example, the Zeeman effect is causing spectral lines to spectrally split under the influence of magnetic fields, and the polarization of the Zeeman components depends on the magnetic field orientation and magnitude. The continuum radiation can in principle also be polarized by a magnetic field (as observed in strongly-magnetized

Further author information: (Send correspondence to F.Z.)
E-mail: franziska.zeuner@irsol.usi.ch

Ground-based and Airborne Instrumentation for Astronomy IX, edited by Christopher J. Evans, Julia J. Bryant, Kentaro Motohara, Proc. of SPIE Vol. 12184, 121840T
 · 0277-786X · doi: 10.1117/12.2629250

white dwarfs, e.g. 3, 4), but this effect is rather negligible on the Sun. Therefore, in solar Zeeman measurements, the continuum is assumed to be unpolarized. However, spectral lines[5] and also the continuum[6,7] can get polarized due to scattering processes in the solar atmosphere, which in the case of Rayleigh scattering is most prominently observed at 90 degree scattering angle, i.e., close to the solar limb.[8] The solar continuum is most notably polarized in the blue, and the entire visible part of the solar spectrum is flooded with scattering polarization in spectral lines. In the presence of magnetic fields, the line scattering polarization can be modified through the Hanle effect[9] (a few examples for solar magnetic fields are given by 10–16), which serves as a valuable diagnostic tool for magnetic fields complementary to the Zeeman effect.

To detect small polarization variations due to the Hanle effect in the solar polarized spectrum, state-of-the-art high-sensitivity polarimetry is essential. Modern solar polarimeters can achieve sensitivities on the order of 0.1%[1] or better[17] within just a couple of seconds exposure time at the resolution limit of the telescope. However, in order to exploit the full potential of Hanle diagnostics, it is necessary to shift from relative to *absolute* polarization measurements with high precision, which requires a dramatic increase of the accuracy of the zero-level determination. Absolute polarization measurements allow for harvesting a valuable information about the solar atmosphere encoded in the continuum polarization,[18] but also for determining Hanle-induced sign-changes in the scattering polarization of spectral lines.[19] Given these examples, it is essential to determine the zero-level of polarization to better than $10^{-4}\,I$.

While the precision of modern sophisticated solar polarimeters are usually limited by statistical shot noise of the photon detection, the polarimetric zero-level accuracy in general is significantly worse than the precision. So far, solar spectropolarimetry focused on improving the accuracy of polarization amplitude determinations and can be as good as $5\cdot10^{-4}\,I_c$,[17] while the *absolute* level of polarization is mostly limited to about $10^{-3}\,I$ (e.g., 20), depending on the telescope and attached polarimeter. Responsible for this limit are systematic errors introduced by a complex train of optical components changing the polarization, like the telescope mirrors[21] or post-focus instruments.

In contrast, some of the night-time astrophysical polarimeters can achieve both the precision and absolute zero-level accuracy at the level of few 10^{-6} (few parts per million[22,23]) thanks to the optimized design, calibration and measurement sequences.[24]

Induced polarization by solar telescopes can be corrected by optimized telescope design (e.g., THEMIS, see 25 and references therein), by complex post-processing data correction schemes[26] or telescope calibration methods.[27,28]

However, due to the overall complexity of solar telescopes, some systematic errors still remain after such corrections and often require additional calibration (see for example 29). As an example, one zero-level calibration technique is based on small-aperture achromatic half-wave plates[30] placed in front of the optical elements to be calibrated. This solution cannot be applied directly to full Stokes measurements. Additionally, the implementation of another optical element in front of the first oblique mirror in the optical train may be technically challenging or unfeasible at existing large aperture telescopes.

In this paper we present a novel technique for measuring solar polarization based on *slow* polarization modulation in combination with the rapidly modulating Zürich IMaging POLarimeter (ZIMPOL[31,32]) allowing for high-precision and high zero-level accuracy full Stokes solar polarimetry at the same time. The novelties consist of using a combination of slowly modulated *full Stokes* measurements *by a zero-order retarder in front of a solar telescope*. The slow modulation is performed by a cost effective rotating zero-order retarder film in front of the Gregory-Coudé telescope in Locarno, Switzerland. This allows to correct the absolute value of the full Stokes vector by minimizing systematic errors. The correction can be performed at wavelengths other than the design wavelength of the zero-order retarder. In particular, after correction the telescope induced polarimetric offsets and especially the cross-talk from circular to linear polarization is significantly reduced, which usually limit the zero-level accuracy of today's polarimeters.

2. SLOW MODULATION: METHOD MOTIVATION AND DESCRIPTION

In the following we describe the instrumental sources that limit the zero-level accuracy of solar polarimetric measurements and describe a measurement technique for correction. We use as an example a specific polarimeter

setup. However, the mathematical description is very general and applicable to any setup where a fast modulating polarimeter is combined with a slow modulation as a first polarimetrically important element. For the mathematical description the Stokes formalism is the most convenient framework to represent the polarization state of natural light and its transformation due to optical elements.

2.1 Limitations of the zero-level accuracy in standard polarimetric measurements

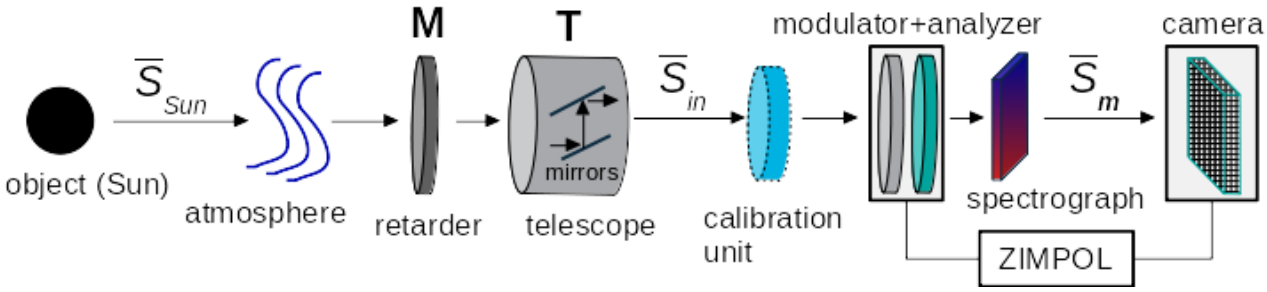

Figure 1. Optical schematic of the slow modulator **M** within the standard optical setup at the IRSOL observatory.

To measure the polarization state of light, most solar polarimeters are based on a (fast) polarimetric modulator and a (synchronized) detector.[1] In the standard polarimetric measurement setup at the 45 cm Gregory-Coudé telescope in the IRSOL observatory (see Fig. 1, without retarder **M**), the ZIMPOL system consists of a fast 42 kHz photo-elastic modulator (PEM), or alternatively a 1 kHz ferroelectric liquid crystal modulator (FLCM), followed by a linear polarizing beam splitter cube (analyzer), synchronized with a demodulating masked CCD detector.[32] The modulator together with the analyzer are mounted on motorized rotary stages to follow the telescope image rotation, which is compensated by a three mirror image de-rotator for a stable image on the spectrograph slit (Czerny-Turner configuration). The modulation is fast enough to minimize spurious polarization signals induced by image motion and blurring from Earth's atmospheric seeing. Such spurious polarization signals constitute a major limitation in the accuracy of ground-based solar polarimetry.[33] Any optical component after the analyzer is calibrated,[34] under the assumption of constant conditions during each modulation cycle.

To calibrate the polarimeter, a polarization calibration unit (a polarizer and an achromatic quarter wave plate to generate predefined Stokes states) is temporary mounted directly after the telescope exit window and precedes the ZIMPOL modulator (see Fig. 1). The calibration procedure is usually applied before scientific measurements. We will not go into the details of this procedure, as it is described in the literature.[35] However, a brief explanation of the concept is given in the following.

Given the $4\times N$ optimum modulation matrix $\mathbf{O}$[36] ($N \geq 4$ for a full Stokes measurement) and an input Stokes 4-vector $\bar{S}_{in}$, the measured intensity N-vector $\bar{I}$ is given by:

$$\bar{I} = \mathbf{O}\bar{S}_{in}. \tag{1}$$

After calibration, which determines the $N \times 4$ demodulation matrix $\mathbf{D}$, the measured Stokes vector $\bar{S}_m$* is assumed to approximate $\bar{S}_{in}$ very well, given the noise in $\bar{I}$ and uncertainties in $\mathbf{D}$:

$$\mathbf{D}\bar{I} = \bar{S}_m \approx \bar{S}_{in}. \tag{2}$$

Optical elements in front of the calibration unit cannot be calibrated for in this way. Due to practical reasons, it is often not possible to place the calibration unit as a first element in the optical train. Also, spurious polarization signals due to the modulator itself cannot be calibrated (e.g., fringes) or if the configuration of optical elements vary with respect to the calibration.

*To be precise, the measured polarization Stokes parameters by ZIMPOL are normalized to the intensity, i.e. $S_{2,m} = Q_m/I_m$. For convenience we omit the explicit writing of the normalization and use $S_{2,m} = Q_m$.

The approximation $\bar{S}_m \approx \bar{S}_{in}$ has some additional limitation, as the calibration for practical reasons has to be temporally separated from the scientific measurement.

One very important limitation is that the polarimetric calibration does not account for instrumental polarization offsets due to the polarizance of optical elements (mostly mirrors) prior in the optical train. At IRSOL, the optical elements in front of the modulator and calibration unit include two flat mirrors under 45° after the secondary mirror and the entrance/exit windows of the telescope tube. The mirrors rotate polarization planes and induce phase shifts, which result in cross-talk, and can induce polarization offsets.

The 4×4 Mueller matrix provides the full characterization of a polarization element.[34] Since the configuration of the two aluminium-coated mirrors inside the telescope to guide the light to the optical laboratory are under oblique angles and their configuration changes slowly over the year,[37] it is difficult to precisely determine the Mueller matrix of the telescope. However, the induced spurious (cross-talk and offset) polarization significantly reduces the zero-level accuracy in polarization measurements, especially close to solstice (polarization offsets up to 10^{-2} in fraction of the intensity are possible).

We denote the telescope Mueller matrix with $\mathbf{T}$, which changes marginally over one day. In the case of a non-diagonal $\mathbf{T}$ (which is only the case for specific times over the year where both mirrors compensate each other), the input $\bar{S}_{in}$ is different from the "true" signal by the Sun, i.e. $\bar{S}_{Sun} \neq \bar{S}_{in} \approx \bar{S}_m$.

We summarize all slowly varying (> 1 min timescale) additional spurious instrumental polarization unrelated to the "real" Stokes $\bar{S}_{Sun}$ signal with $\Delta\bar{S}$ (e.g., temporally stable fringes as in FLC modulators). Then,

$$\bar{S}_m = \mathbf{T}\bar{S}_{Sun} + \Delta\bar{S}. \tag{3}$$

Note that $\bar{S}_{Sun}$ is partially polarized, meaning that the Stokes vector is composed of a polarized and an unpolarized part. The polarized part in combination with $\mathbf{T}$ will result in polarimetric cross-talk, while the unpolarized part[†] will get partially polarized and adds polarimetric offsets.

2.2 Slow modulation scheme

In order to minimize the mentioned static errors decreasing the zero-level accuracy in polarimetric measurements, we employ an additional *slow modulation* with a birefringent zero-order retarder before any optical element influencing the polarization. The ideal retarder has a Mueller matrix $\mathbf{M}(\theta, \delta)$, depending on the phase shift δ and the orientation angle θ, for the full matrix see equation 17 in the Appendix 6.1. Therefore, by adding the retarder to the telescope entrance, the relationship between the measured and incoming beam changed from equation 3 to (neglecting photon noise contributions)

$$\bar{S}_m = \mathbf{T}\mathbf{M}(\theta, \delta)\bar{S}_{Sun} + \Delta\bar{S}. \tag{4}$$

The slow modulation scheme is given by four angles per slow modulation cycle, which are $\theta_1 = 0°, \theta_2 = 45°, \theta_3 = 90°, \theta_4 = 135°$. Therefore, for the ith measurement within the slow modulation cycle ($\mathbf{M}_i = \mathbf{M}(\theta_i, \delta)$):

$$\bar{S}_{m,i} = \mathbf{T}\mathbf{M}_i\bar{S}_{Sun} + \Delta\bar{S}. \tag{5}$$

One assumption is that $\mathbf{T}$, $\bar{S}_{Sun}$ and $\Delta\bar{S}$ stay constant, i.e. they are time independent within one slow modulation cycle.

A zero-order retarder has a well-defined design wavelength where it induces a phase shift of π (retardance $r = \frac{\delta}{2\pi}$ of 0.5) and acts as a half-wave plate, while at a different wavelength the phase shift is $\frac{\pi}{2}$ ($r = 0.25$, a quarter-wave plate). Hence, a maximum polarimetric efficiency for the linear polarization states and circular polarization is achieved when working at a wavelength where the retarder induces a half-wave shift and a quarter-wave phase shift, respectively. However, when operating at other wavelengths than these two specific ones, both linear and circular polarized light is modulated. We explore the dependency of the polarimetric efficiency dependent on the wavelength in Sect. 2.2.4.

[†] $\bar{S} = (I, Q, U, V)^T = (I - \sqrt{Q^2 + U^2 + V^2}, 0, 0, 0)^T + (\sqrt{Q^2 + U^2 + V^2}, Q, U, V)^T$

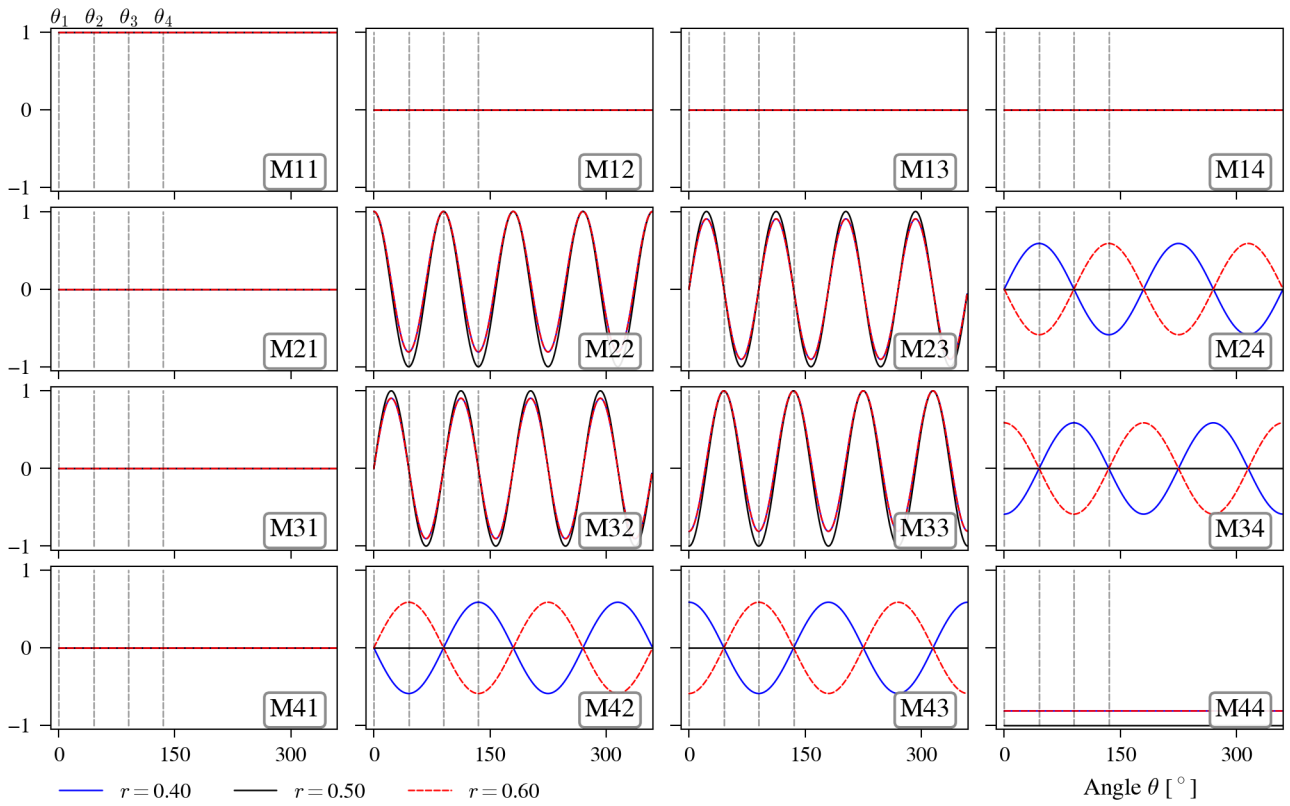

Figure 2. Mueller matrix elements of an ideal retarder for three different retardance values r in dependence of orientation angle θ. Note that for $r \neq 0.5$ cross-talk elements V to Q and U appear. Vertical dashed lines indicate the four positions of the slow modulation cycle.

As we show in Fig. 2, a minimum of the four angles introduced above are necessary in order to account for additional cross-talk terms induced by the retarder when used at wavelengths outside the half wave design wavelength. Interestingly, these cross-talk terms show a sign change for retarder orientation angles which are 90° apart.

We use this circumstance to combine in a specific way the full Stokes vectors $\bar{S}_{m,i}$ obtained during the slow modulation cycle to minimize not only static errors (at the time scale of the slow modulation cycle), but also remove additional cross-talk by the retarder at wavelengths other than the design wavelength. In this way, it is possible using a half-(or quarter-)wave retarder to increase the zero-level accuracy in polarimetric measurements in a wide wavelength range and almost independently of the design wavelength. In the following, we describe the correction scheme, i.e. how to combine the Stokes measurements obtained during the slow modulation. Since all four Stokes parameters are already given by the fast demodulation (in our case, the calibrated ZIMPOL images), we call this additional combination "pseudo"-demodulation. The modulation scheme is the same for the linear and circular polarization states, but the "pseudo"-demodulation scheme depends on the polarization state desired to be corrected.

2.2.1 "Pseudo"-demodulation for the linear polarization states

In order to correct the linear polarization states, we combine the four slow modulation measurements with

$$\bar{S}_{m,1} - \bar{S}_{m,2} + \bar{S}_{m,3} - \bar{S}_{m,4} = \mathbf{T}\underbrace{(\mathbf{M}_1 - \mathbf{M}_2 + \mathbf{M}_3 - \mathbf{M}_4)}_{=\mathbf{K}}\bar{S}_{Sun} + \underbrace{\Delta\bar{S} - \Delta\bar{S} + \Delta\bar{S} - \Delta\bar{S}}_{=0}. \quad (6)$$

It is immediately clear that this combination removes the static errors $\Delta\bar{S}$, i.e. temporally stable fringes

by the fast modulator. By combining the measurements in this way, the matrix $\mathbf{K}$ is diagonal (we show this explicitly in Appendix 6.1.1) with $K_{11} = K_{44} = 0$, and $K_{22} = -K_{33} = 2 \cdot (1 - \cos\delta)$. Then:

$$\bar{S}_{m,1} - \bar{S}_{m,2} + \bar{S}_{m,3} - \bar{S}_{m,4} = K_{22} \begin{pmatrix} 0 & T_{12} & -T_{13} & 0 \\ 0 & T_{22} & -T_{23} & 0 \\ 0 & T_{32} & -T_{33} & 0 \\ 0 & T_{42} & -T_{43} & 0 \end{pmatrix} \bar{S}_{Sun}. \tag{7}$$

This removes the circular to linear polarization cross-talk and the telescope induced polarimetric offsets, since the first and last columns are zero.

It is important to note that this correction does not remove $Q \leftrightarrow U$ cross-talk. For the IRSOL Gregory-Coudé telescope, the telescope Mueller matrix elements $|T_{22}| = |T_{33}| \approx 1$ while $|T_{23}| = |T_{32}| \ll 1$. However, close to solstice the latter elements can be significant.[38] Neglecting the $Q \leftrightarrow U$ cross-talk, to recover the linear polarization states of $\bar{S}_{Sun}$, the left hand side of equation 7 is divided by K_{22}:

$$\begin{aligned} Q_{Sun} &\approx \frac{1}{2}(1 - \cos\delta)^{-1}(Q_{m,1} - Q_{m,2} + Q_{m,3} - Q_{m,4}) \\ U_{Sun} &\approx -\frac{1}{2}(1 - \cos\delta)^{-1}(U_{m,1} - U_{m,2} + U_{m,3} - U_{m,4}) \end{aligned} \tag{8}$$

Note that the slowly modulated Stokes parameters Q_m and U_m are normalized with the cosine of the retardance r, which results in efficiency loss of the measurements for $r \neq 0.5$. This aspect is further investigated in Sect. 2.2.4. The retardance for a zero-order retarder only dependents on the wavelength, but despite the efficiency loss the "pseudo"-demodulation and resulting correction is wavelength independent.

Since the (ideal) retarder does not modulate the intensity, combining the intensity Stokes parameters $I_{m,i}$ as described before results in zero. Therefore, the intensity has to be handled separately, for example averaging all intensities of the slow modulation cycle:

$$I_{tot} = \frac{1}{4}\sum_{i=1}^{4} I_{m,i}. \tag{9}$$

The same procedure can be used for the circular polarization for measurements where only the linear polarization is corrected, for example if the efficiency for the circular polarization is too low (i.e. $r \approx 0.5$, see Sect. 2.2.4 for the definition of the efficiency):

$$V_{tot} = \frac{1}{4}\sum_{i=1}^{4} V_{m,i}. \tag{10}$$

2.2.2 "Pseudo"-demodulation for the circular polarization state

A different combination of the slowly modulated Stokes parameters is used to recover V_{Sun}, for wavelengths where $r \neq 0.5$. Combining the four measurements with

$$-\bar{S}_{m,1} + \bar{S}_{m,2} + \bar{S}_{m,3} - \bar{S}_{m,4} = \mathbf{T}\underbrace{(-\mathbf{M}_1 + \mathbf{M}_2 + \mathbf{M}_3 - \mathbf{M}_4)}_{=\mathbf{L}}\bar{S}_{Sun} + \underbrace{(-\Delta\bar{S} + \Delta\bar{S} + \Delta\bar{S} - \Delta\bar{S})}_{=0} \tag{11}$$

removes (analogously to the linear polarization case) the static errors due to the alternating sign of the combination. We derive the matrix $\mathbf{L}$ in Appendix 6.1.2.

Due to the telescope Mueller matrix and the non-diagonal matrix $\mathbf{L}$, there are more residual cross-talk elements than in the linear polarization case:

$$-\bar{S}_{m,1}+\bar{S}_{m,2}+\bar{S}_{m,3}-\bar{S}_{m,4}=L_{24}\begin{pmatrix}0 & -T_{14} & -T_{14} & T_{12}+T_{13}\\ 0 & -T_{24} & -T_{24} & T_{22}+T_{23}\\ 0 & -T_{34} & -T_{34} & T_{32}+T_{33}\\ 0 & -T_{44} & -T_{44} & T_{42}+T_{43}\end{pmatrix}\bar{S}_{Sun}, \tag{12}$$

but the telescope polarimetric offsets are removed (first column is zero). Close to equinox, $|T_{23}|=|T_{32}|\ll 1$ and $|T_{24}|\approx|T_{34}|\approx 0$ holds for the IRSOL telescope. Then, with $L_{24}=2\cdot\sin\delta$, the circular polarization V_{Sun} can be recovered from either the measured Stokes $Q_{m,i}$ or $U_{m,i}$.

To increase the signal-to-noise, both measured linear polarization states can be averaged, therefore the final expression for the circular polarization is:

$$V_{Sun}\approx\frac{1}{4}(\sin\delta)^{-1}(-Q_{m,1}+Q_{m,2}+Q_{m,3}-Q_{m,4}-U_{m,1}+U_{m,2}+U_{m,3}-U_{m,4}) \tag{13}$$

2.2.3 "Pseudo"-demodulation to correct full Stokes

For an efficient full Stokes correction it is necessary that $r\neq 0.5$ and $r\neq 0.25$. Writing the four measured Stokes vectors during the slow modulation cycle with $\bar{S}_{sm}=(\bar{S}_{m,1},\bar{S}_{m,2},\bar{S}_{m,3},\bar{S}_{m,4})^{\mathrm{T}}$ the recovered Stokes vector of the Sun is $\bar{S}_{Sun}\approx\mathbf{P}\bar{S}_{sm}$, $\mathbf{P}$ being a 4×16 matrix. With the "pseudo"-demodulation schemes given in the previous two sections, i.e. equations 8, 9 and 13, the "pseudo"-demodulation matrix is

$$\mathbf{P}=\begin{pmatrix}a & 0 & 0 & 0 & a & 0 & 0 & 0 & a & 0 & 0 & 0 & a & 0 & 0 & 0\\ 0 & b & 0 & 0 & 0 & -b & 0 & 0 & 0 & b & 0 & 0 & 0 & -b & 0 & 0\\ 0 & 0 & -b & 0 & 0 & 0 & b & 0 & 0 & 0 & -b & 0 & 0 & 0 & b & 0\\ 0 & -c & -c & 0 & 0 & c & c & 0 & 0 & c & c & 0 & 0 & -c & -c & 0\end{pmatrix} \tag{14}$$

with $a=\frac{1}{4}$, $b=\frac{1}{2}(1-\cos\delta)^{-1}$ and $c=\frac{1}{4}(\sin\delta)^{-1}$.

2.2.4 Polarimetric efficiency

Intensity measurements have a signal-to-noise-ratio (SNR) depending on the number of available photons, given that the measurements are photon shot noise limited. For polarimetry, modulated intensity images need to be combined to recover the polarimetric Stokes parameters Q,U and V. Depending on the efficiency of the modulation, the SNR might be reduced. We will now define the efficiencies for the slow modulation scheme shown in the section before. Since the slow modulation works with the fast demodulated Stokes parameters, there is an additional efficiency reduction (depending on the fast modulation not considered here).

Based on the definition given by 34, the efficiency ξ_i of the recovered Stokes parameter i after slow demodulation is given by the elements of the demodulation matrix $\mathbf{P}$ (with 16=4×4 measurements, but four of them "simultaneously" with the FLCM setup)

$$\xi_i=\left(4\sum_{j=1}^{16}P_{ij}^2\right)^{-1/2} \tag{15}$$

The efficiencies for the three polarization states are therefore

$$\begin{aligned}\xi_Q&=\left(4\sum_{j=1}^{16}P_{2j}^2\right)^{-1/2}=\xi_U=\left(4\sum_{j=1}^{16}P_{3j}^2\right)^{-1/2}=\frac{1}{2}(1-\cos\delta)\\ \xi_V&=\left(4\sum_{j=1}^{16}P_{4j}^2\right)^{-1/2}=\sin\delta.\end{aligned} \tag{16}$$

We plot the efficiencies with respect to the wavelength for one example retarder in Fig. 3.

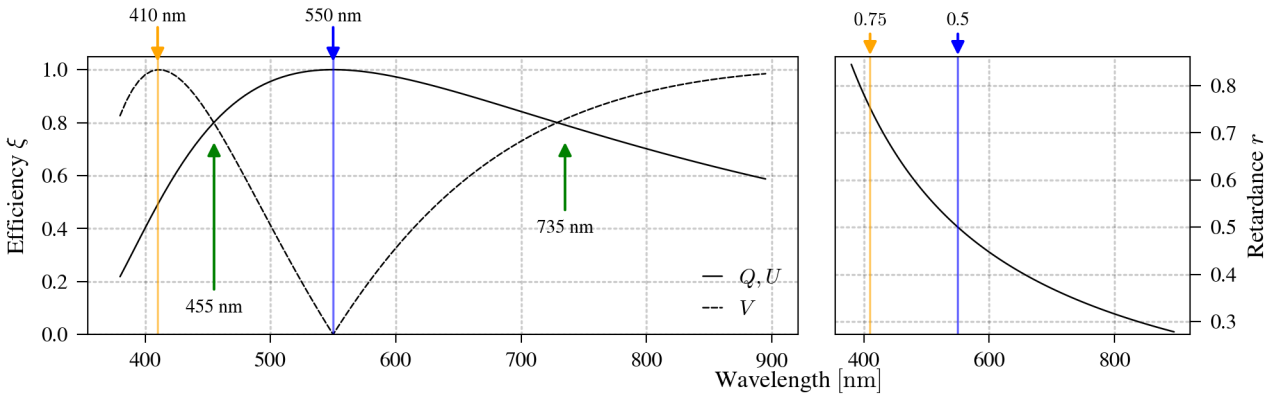

Figure 3. Polarimetric efficiencies (left panel) and measured retardance (right panel) for one retarder film at IRSOL. The film is a half-wave retarder at 550 nm (blue line) and a quarter-wave retarder at 410 nm (orange line). Green arrows indicate the wavelengths of balanced efficiencies for the circular and linear polarization.

For the full Stokes correction the efficiencies are balanced where $\xi_V(r_F) = \xi_{Q,U}(r_F)$, this is, where $r_F \approx \{0.35, 0.65\}$. The above sections demonstrate that the correction works in principle quite independently of the retardance. However, the retardance is included in the corrected Stokes parameters as a scaling factor, and may reduce the accuracy of the measured polarimetric amplitude, if not well known. This aspect is investigated in Sect. 4, however, the optimization of the amplitude accuracy is out of the scope of this paper.

3. THE SLOW MODULATOR SETUP AT IRSOL

The realization of the slow modulation setup at the IRSOL observatory is shown in Fig. 4.

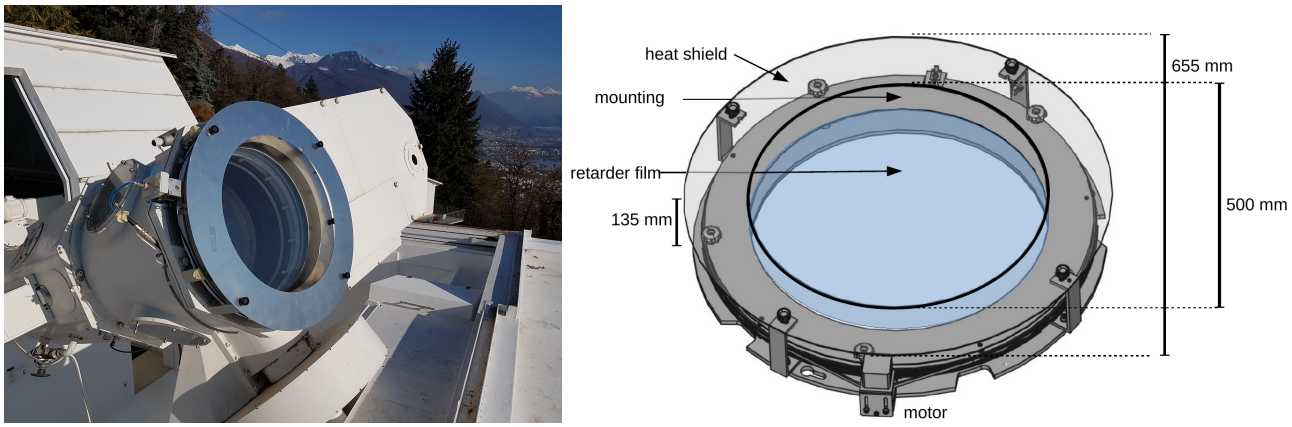

(a) (b)

Figure 4. The slow modulator at the IRSOL observatory. (a) When it is mounted to the IRSOL telescope, the retarder film covers the complete telescope aperture. (b) Technical drawing with dimensions of the slow modulator.

As mentioned in the last section, the retarder has to be mounted before any oblique telescope mirrors. For the IRSOL telescope, there are only two options: either inside the vacuum tube after the secondary mirror or in front of the telescope entrance. The first option poses a major challenge in terms of mounting and feasibility to change the components regularly. Therefore, the second option was explored, which requires a large diameter half-wave plate. Achromatic half-wave plates with diameters in the order of 0.1 m can achieve a high optical quality and retardance uniformity,[39] but for larger diameters performance requirements have to be relaxed for a low budget solution. Therefore, a chromatic zero-order retarder film with lower optical quality is used in order to cover the full 0.45 m telescope entrance. Since the telescope in combination with ZIMPOL does not allow for spatial resolutions higher than $\sim$ 1.3 arcsec, the main scientific focus of observations is not high

resolution but high polarimetric sensitivity. Thus, the potential resolution degradation using a retarder film with relaxed requirements is acceptable. In the following we describe the design and components of the complete slow modulation setup at IRSOL.

The slow modulator consist of two main components: the motorized rotation stage (a large, but light, ball bearing moved by a step motor with high precision ($< 0.1°$). and a zero-order retarder film. Several retarder films with different design wavelengths are available. The two mainly used retarder at IRSOL are a half-wave and a quarter-wave retarder film at 550 nm and 646 nm, respectively. The spectral working ranges given in Table 1 are where the efficiency (see Sect. 2.2.4 for definition) is above 0.4 for all Stokes parameters. Figure 4 panel (b) shows the technical layout of the slow modulator. The retarder films are low cost and commercially available components[‡]. The free aperture of the slow modulator is about 45 cm in diameter and it is placed close to the telescope entrance window.

The orientation of the optical fast axis was calibrated by minimizing $Q \leftrightarrow U$ cross-talk where only Q is expected from the Sun, i.e. the scattering polarization signal parallel to the solar limb very close to equinox. The measurement error for the retarder orientation angle with this method is about 0.5°.

The retardance was measured as a function of the wavelength, see Fig. 3. Given the large dimensions of the film, only small samples (few centimeters in diameter) from four different edge locations were possible to be measured. The estimated variation of the retardance based on these different sample locations is about 0.3%. Due to small number of samples, this retardance variation can only serve as a lower limit, and realistically the retardance variation is expected to be higher. The variation of the retardance may introduce additional noise due to slightly varying modulation efficiencies. Thermal changes and gradients may introduce retardance variation as well.[39] Since the transmission of the retarder is high (see Table 1), the retarder temperature is practically the same as the environment temperature (outside the telescope) without major temperature gradients. However, over the day, the outside temperature can vary a few degrees and therefore is not very stable. We do not consider this a major limitation, as during one slow modulation cycle the retarder temperature is expected to be stable. Although here we are not focusing to optimize the polarimetric amplitude accuracy, we study the effect of several retardance variations on the amplitude uncertainty in Sect. 4.4.

It is expected that due to the vast size of the retarder film the thickness variations (potential source of wavefront errors) may result in a lower image quality. Given the seeing conditions at IRSOL we have not been able to quantify an image quality loss or a reduction of spatial resolution when the slow modulator is used. Table 1 compiles the main specifications of the slow modulator retarder film.

Table 1. Technical specifications of the retarder films.

Retarder specification	Value
Retarder film 0.5@550 nm, spectral working range	400-500 and 610-900 nm
Retarder film 0.25@646 nm, spectral working range	450-710 nm
Transmission	$\sim 90\%$
Material	Polycarbonate, smoothed, uncoated
Thickness	0.07 mm $\pm$ 0.046 mm
Retardance variation Δr	$\pm$ 0.3 %
Optical axis orientation error θ_{offset}	$\sim 0.5°$
Heat damage threshold	85° C (low to very low humidity)

In the next section we discuss the results obtained using this slow modulator setup with the modulation scheme presented in Sect. 2.

4. ACTUAL PERFORMANCE AND LIMITATIONS

The performance of the slow modulation method has been tested at several wavelengths in the visible and with both fast modulators available at IRSOL. Here, we present the results at a selection of wavelengths. In practice,

[‡]American Polarizers Inc., https://www.apioptics.com/.

the new technique has been successfully applied in the wavelength range 380–700 nm.[18] While for the FLCM the slow modulation and demodulation scheme presented in Sect. 2 can be applied directly, a small modification of both is needed when using the PEM. The combination of ZIMPOL with the PEM is able to measure only three Stokes parameters at the same time (e.g., I, Q, V). In standard full Stokes measurements, the orientation of the PEM is therefore alternating between 0° and 45° to measure I, Q, V and I, U, V consecutively.[40] However, the optical thickness of the PEM may result in a small beam wobble. We decided to take advantage of the additional slow modulation and instead of rotating the PEM having a second slow measurement sequence with the angles $\theta_5 = 22.5°, \theta_6 = 67.5°, \theta_7 = 112.5°$ and $\theta_8 = 157.5°$. Therefore for the slow modulation with the PEM there are eight angle positions instead of four, which are analogously demodulated as described in Sect. 2. In practice, the retarder angles for the PEM and the FLCM are not restricted to the first half of the circle (i.e., $\theta < 180°$), which means that the retarder can be unlimitedly rotated. This has also the advantage of reducing spurious systematic errors introduced by the retarder itself, as we will show later in this section.

In the following we present the results of the test measurements as well as the found limitations of the slow modulation method applied at the IRSOL observatory, using the retarder film which has a retardence of 0.5 at 550 nm.

4.1 Linear polarization correction

We show an example for an uncorrected (without slow modulation) Stokes measurement with the PEM in Fig. 5. The measurement was conducted at the solar disk center in a region with low magnetic activity (only a few small-scale magnetic concentrations were present).

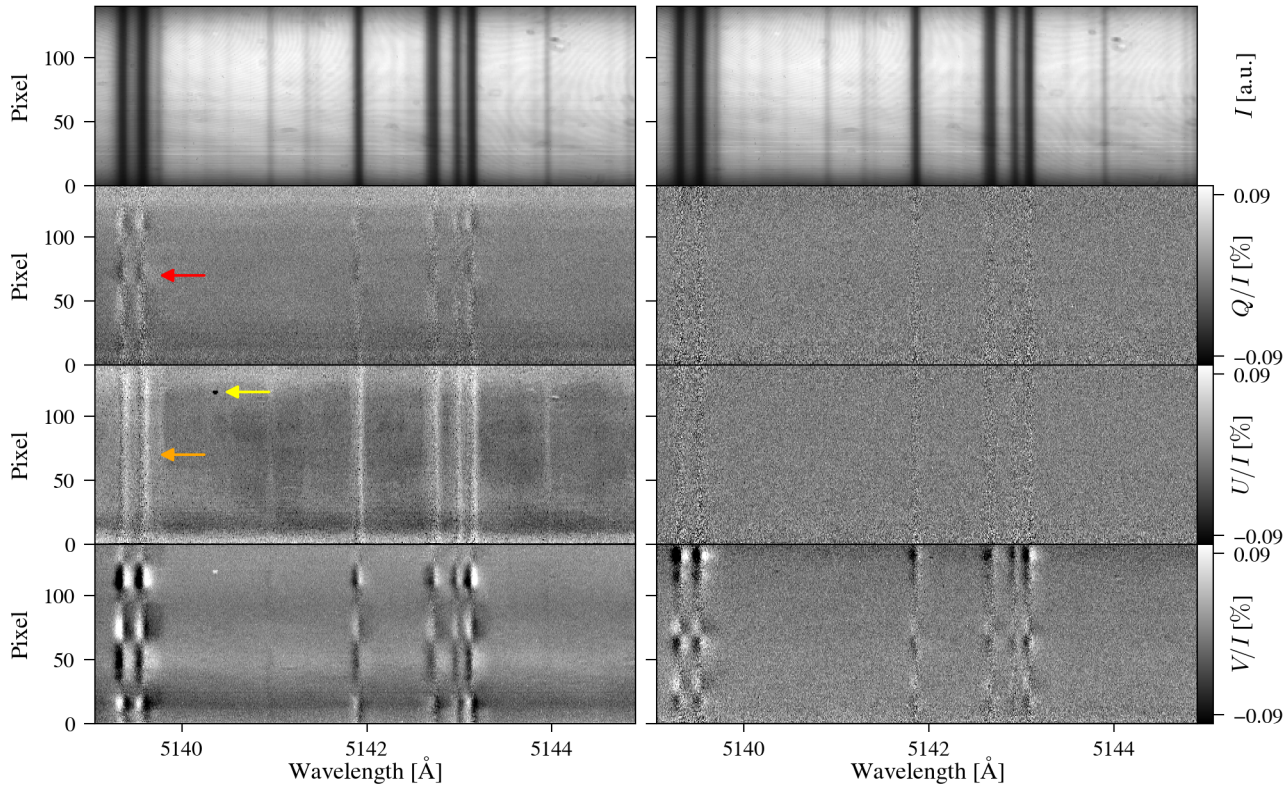

Figure 5. ZIMPOL full Stokes measurement with the PEM at the solar disk center without (left, the mean is subtracted) and with (right) slow modulator on the same day. Detector errors (yellow arrow), cross-talk $I \rightarrow U/I$ (orange arrow) and $V/I \rightarrow Q/I$ (red arrow) are visible in the left panel. The grey scale applies to both panels.

Hence, linear polarization signals in the spectral lines are expected to be very small and the continuum is polarization free. The circular polarization is present due to magnetic field concentrations. The data was reduced using the basic standard ZIMPOL reduction pipeline, which includes a dark frame correction and a polarimetric calibration, but removal of fringes was not carried out.

There are many artifacts visible in Fig. 5: detector errors, well-visible cross-talk from Stokes I and V/I to linear polarization, and additional polarimetric offsets on the order of $10^{-2}I$ in U/I.

These artifacts are reduced significantly when the slow modulator is used. The correction was done by combining polarimetrically calibrated ZIMPOL data described in the Sect. 2.2.1. Stokes V/I is not corrected and processed as given by equation 10.

For a comparison between the uncorrected and corrected data, the measurements were taken at the same day and we made sure that the photon statistics were comparable in both measurements, i.e. the number of accumulated frames and the exposure times were the same. No additional post-processing, such as removal of fringes was applied. The offsets in the corrected linear polarization was as small as a few $10^{-6}I$. Interestingly, the artifacts in Stokes V/I appear to be reduced in the slowly modulated observation although there is no correction applied. We suspect some of the background effects are a consequence of a beam wobble introduced by the PEM when it has to be rotated to measure Q/I and U/I. Since this rotation is omitted when the slow modulation technique is used, the background effects are less pronounced.

4.2 Full Stokes correction

As a next step, we give an example of a full Stokes correction.

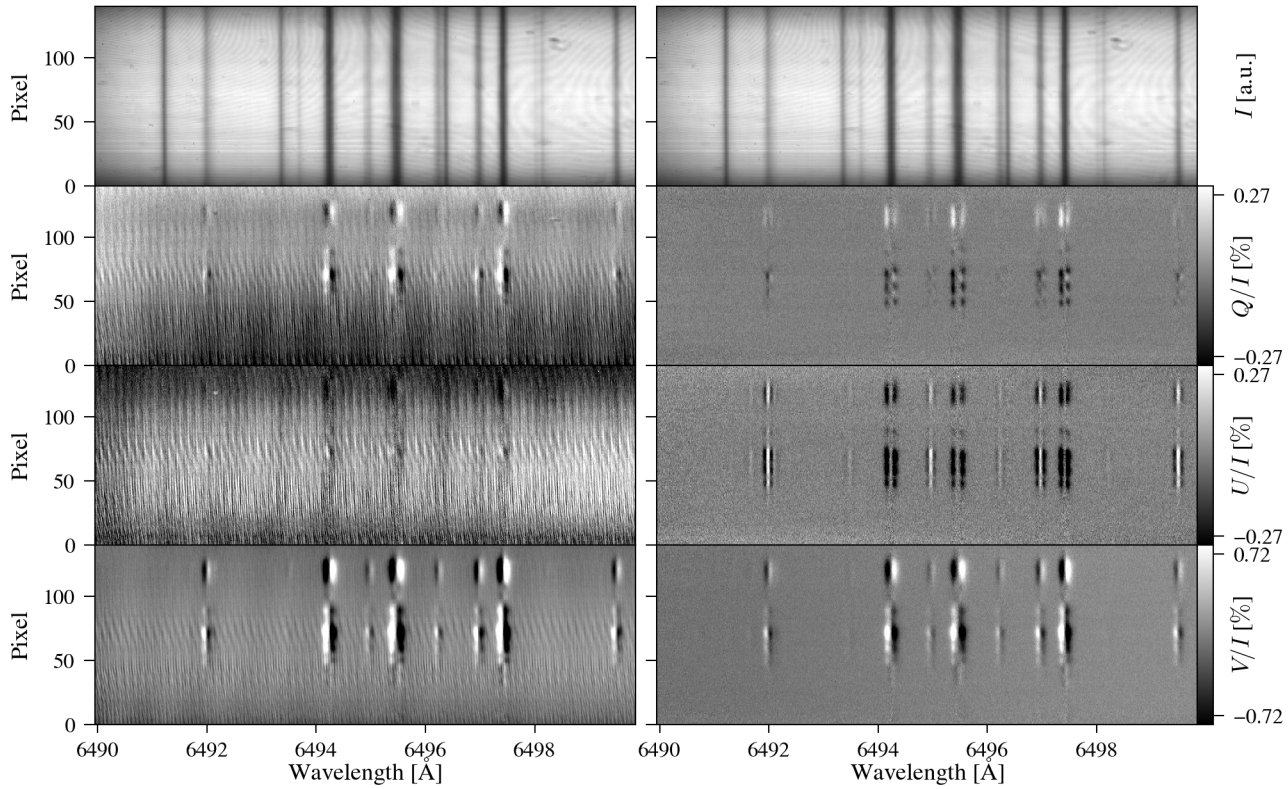

Figure 6. ZIMPOL full Stokes measurement with the FLCM of a pore without (left, the mean is subtracted) and with (right) slow modulator correction on the same day. The grey scale applies to both panels.

For the next example we used ZIMPOL together with the FLC modulator. The wavelength region to test the correction by applying the slow modulation was chosen to be high in efficiency ($\xi > 0.5$) for all three polarization Stokes parameters (i.e., 649 nm, see Fig. 3 for efficiencies). We observed a pore, which produces significant linear and circular polarization in spectral lines. In the left panel of Fig. 6 the ZIMPOL images without the correction applied are shown. Here the strongly polarized fringes are prominently visible as well as cross-talk from Stokes V/I to the linear polarization states. When the "pseudo"-demodulation presented in Sect. 2.2.3 is applied, both artifacts are significantly suppressed. The successful correction of the cross-talk is evident from the symmetric linear polarization profiles (as expected due to the Zeeman effect) in the right panel of Fig. 6. The effect of fringes are reduced to below the noise level.

4.3 Residual background and offsets

Some observations before the correction show significant large scale variations of the background in spatial and spectral direction, for an example see U/I in Fig. 5.

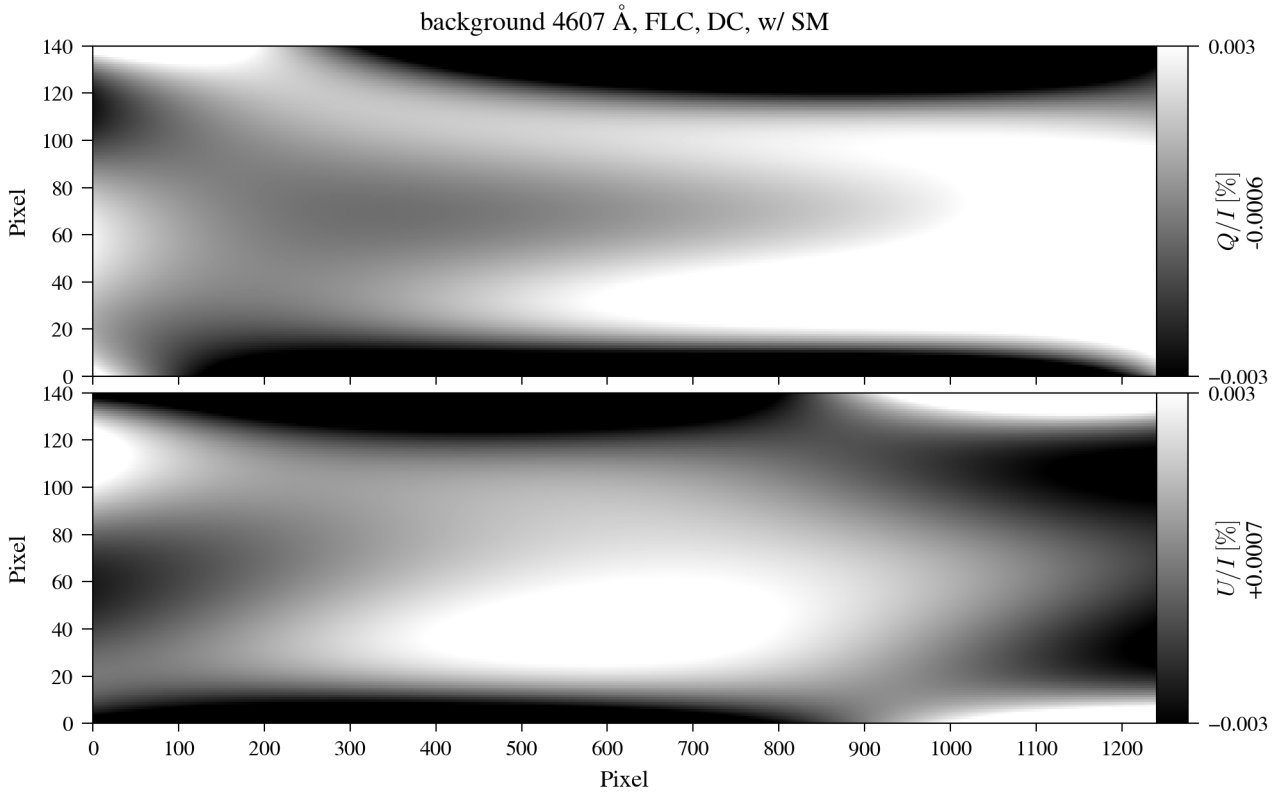

Figure 7. Example of the residual background variation of a measurement in the Sr I 4607 Å region observed in a quiet Sun region at disk center with the slow modulator. The number below the scale labeling corresponds to the mean subtracted from the background image.

Such background variations and polarimetric offsets affect the zero-level accuracy. While the latter is the result of telescope induced polarization, the first is of yet unknown origin. One possible scenario is that the de-rotator, which compensates the image rotation on the slit, may introduce these effects, since it is constantly rotating, but also imperfect pre-filter for the spectrograph may introduce spectral variation. As this is severe for scattering polarization measurements, we will focus in the following to the two linear polarization states.

To investigate the residual background variations and offsets, we observed at several wavelength regions with both modulators at solar disk center in a quiet Sun region, where a minimum of solar polarization is expected. The wavelength positions are chosen to be close to scientifically interesting spectral lines polarized by scattering

processes. We took care that the photon statistics are comparable between the measurements with and without the slow modulator, and at least not too different at different wavelength positions. The integration times were on the order of about 20 min. The measurements with and without the slow modulator are obtained at the same day.

An example of the large-scale varying residual background is shown in Fig. 7, which is the result from fitting 2D polynomials of 3rd order to the Stokes Q/I and U/I images to isolate the background from the spectral lines. We calculate the RMS (root-mean-square) of this background, and compare them for all measured wavelengths and modulators in Fig. 8. The background variation is generally larger in the case of the FLCM, as the PEM is expected to have a better optical quality. Since we multiply the RMS of the measurements with the slow modulation (SM, shown with solid circles) by 10, it is clear that the new measurement method reduces the RMS of the background by a factor of about 10, in most cases even more. The least improvement is found in the red with the PEM, where there is a reduction of a factor 5. The background variation RMS has no obvious dependency on the wavelength or modulator. Reduction of the background RMS works very well with the slow modulation technique and the worst-case residual background variations are on the order of $2 \cdot 10^{-5} I$ and $10^{-4} I$ for the PEM and FLCM, respectively.

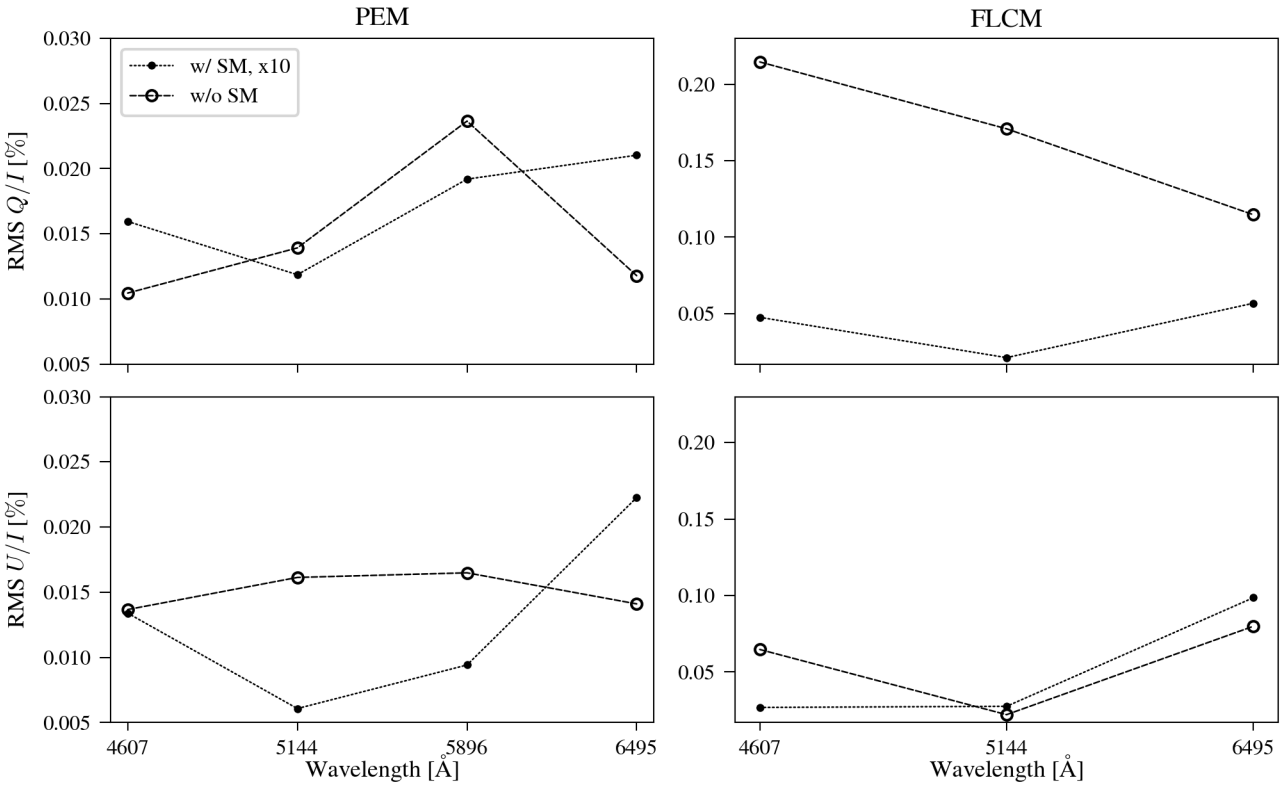

Figure 8. RMS of the smoothed background in the linear polarization images at various wavelengths with both modulators (PEM: left panels, FLCM: right panels), with and without the slow modulator (SM). Note that the values for the measurements with the slow modulation are multiplied by 10.

To estimate the residuals on the polarimetric offsets the spatial averages over the Stokes Q/I and U/I images are calculated. The offsets are compiled in Table 2. The improvement of the zero-level accuracy with the slow modulation method can reach a few orders of magnitude. Under good and stable conditions we can reach absolute precisions on the order of $\lesssim 2 \cdot 10^{-5}\, I$ and $\lesssim 5 \cdot 10^{-5}\, I$ for the PEM and FLCM, respectively.

Table 2. Offsets for different wavelengths and modulators with and without applying the slow modulation. Values are given in %.

Wavelength [Å]	4607		5144		5896		6495	
Stokes [/I]	Q	U	Q	U	Q	U	Q	U
PEM	1.0977	0.8600	0.1561	0.05810	0.0704	0.1182	0.4703	0.5862
PEM, w/ SM	0.0013	0.0012	0.0006	0.0008	0.0006	0.0006	0.0009	0.0009
FLCM	1.1768	3.3625	1.3592	2.8821	-	-	1.9076	3.5672
FLCM, w/ SM	0.0022	0.0020	0.0020	0.0016	-	-	0.0037	0.0054

In Fig. 9 the offsets are plotted considering either the first, second or both halves of the retarder for modulation for several cycles. Only in the last case the offset is reducing as expected if shot noise limited (i.e., the offset of N cycles follows the curve which scales the offset of the first measurement with $\sqrt{N}$). Hence, the precision of the zero-level accuracy is shot noise limited when the retarder is rotated in complete turns.

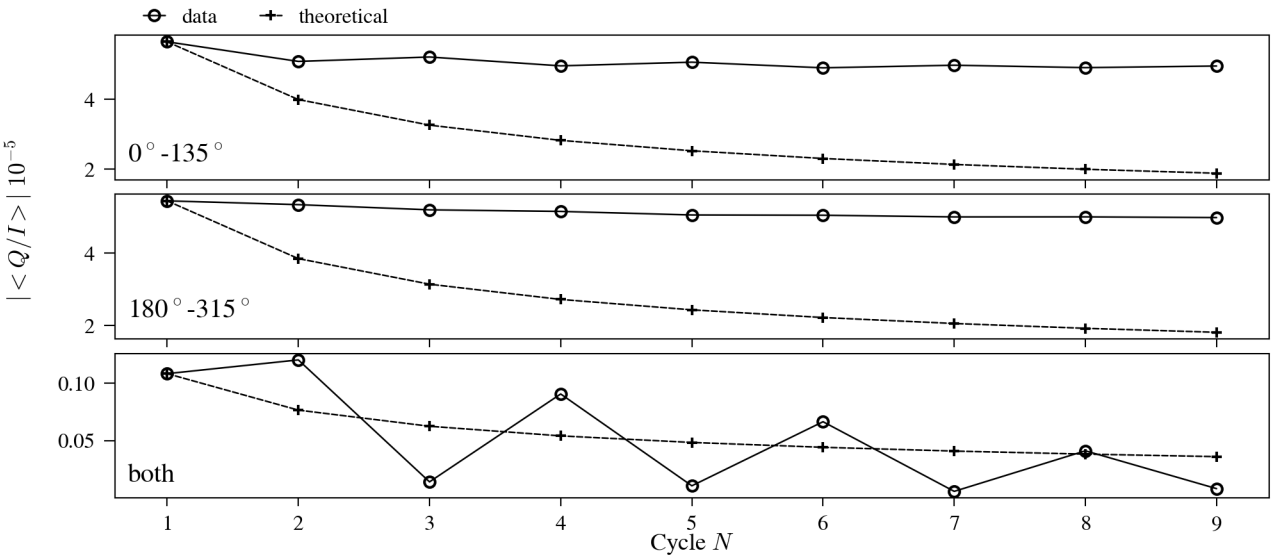

Figure 9. Observed and theoretically expected residual offsets in Q/I for the average of N slow modulation cycles. Top panel: only cycles of the first half of the retarder are averaged. Center panel: only cycles of the second half of the retarder are averaged. Bottom panel: full turns are averaged.

4.4 Estimation of polarization amplitude uncertainty

Although it is not the focus of this work to maximize the polarization amplitude accuracy, we study here the impact of the main parameters of the slow modulation method on the amplitude accuracy. The measured (see Sect. 3) retardance of the standard retarder film at various wavelengths has been tested by measuring the scattering polarization amplitude at the solar limb with and without the slow modulator, and comparing the amplitudes. They have been found to be similar within a 1-2%.

The main parameters influencing the polarization amplitude accuracy are the precision of the retarder rotation $\Delta\theta$ and the retardance variation Δr. To estimate their influence on the amplitude uncertainty we simulate an ideal measurement (without considering any noise or additional systematic errors) 10000 times given an arbitrary, fixed polarization amplitude (1% for linear and 10% for circular) and a fixed retardance r and fixed retarder position angles plus a random offset from a Gaussian distribution with either $\Delta\theta$ or Δr as a standard deviation for the angle position and retardance precision, respectively. The demodulation is performed by using the fixed retardance r. The histogram of the difference between the fixed polarization amplitude and the demodulated polarization amplitude is fitted by a Gaussian. The standard deviations of these fitted Gaussians are shown in Fig. 10 and are an estimation of the polarization amplitude uncertainty resulting from retardance and retarder position errors. Vertical dashed lines represent the estimated errors of the standard retarder film at IRSOL.

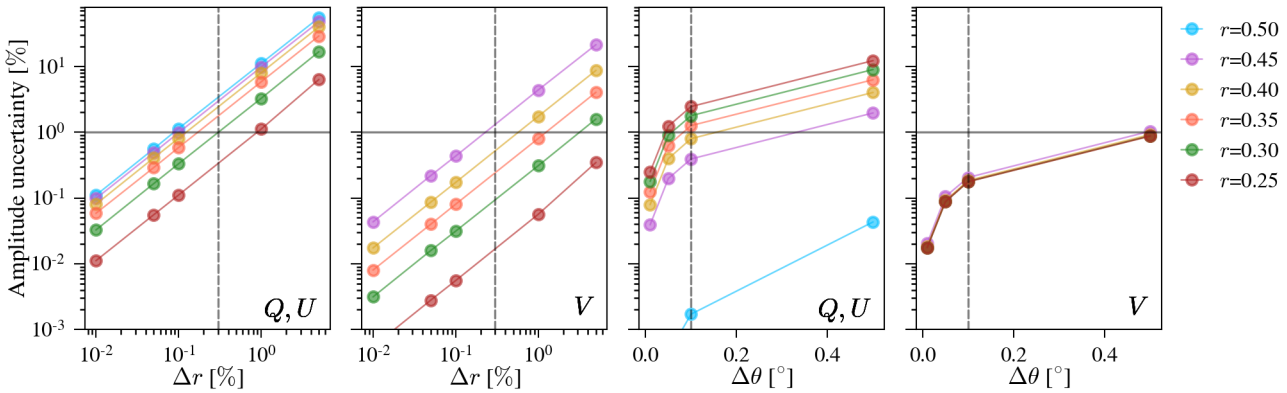

Figure 10. Polarization amplitude uncertainty given a retardance variation. Polarization amplitude uncertainty given a retarder position angle precision.

The circular polarization amplitude is less sensitive to both error sources (unless the measurement is performed very close to a wavelength where the retarder induces a half wave phase shift) than the linear polarization amplitude. This is because the uncertainty is given in percent, and the circular polarization amplitude is usually larger than the linear polarization amplitude, therefore the error percentage is smaller. Given the errors assumed for the standard retarder film at IRSOL, the maximum amplitude uncertainty for the linear polarization is 2%, which is what has been estimated from observations.

If the retarder has an angle offset due to an imperfect alignment of the fast axis, this results in an additional cross-talk between the linear polarization states. Since the alignment of the retarder has been performed by minimizing the cross-talk between Stokes Q and U, the precision of the optical axis orientation is limited by the cross-talk measurement. We estimated our alignment to not be better than 0.5°, resulting in potentially $Q \leftrightarrow U$ cross-talk with the slow modulation on the order of 2-3%, see Fig. 11.

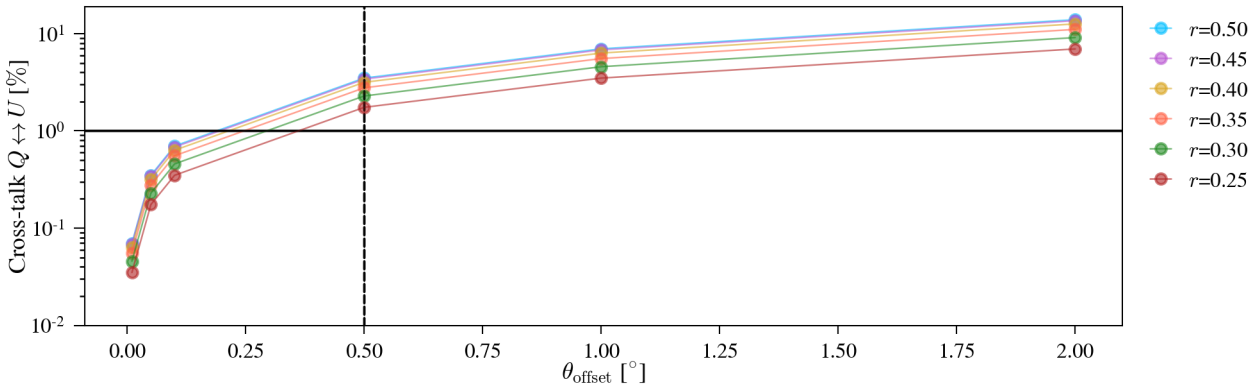

Figure 11. Cross-talk percentage given an angle offset.

5. DISCUSSION AND CONCLUSIONS

We have investigated a new measurement technique for ground-based solar polarimetry based on coalescing a slow modulator placed in front of the telescope with a high-sensitivity full Stokes polarimeter at the IRSOL observatory. The technique reduces slowly varying systematic instrumental errors, including telescope ones (due to its position in front of the telescope), which significantly enhances the zero-level accuracy by orders of magnitude. For the implementation of the slow modulation a large diameter commercially available zero-order retarder film is used. Taking into account the technical feasibility at the IRSOL observatory, the straightforward and low-cost implementation, this technique is superior to the standard solar polarization measurement technique,

which often require additional calibration procedures or elaborate analysis to correct for errors like telescope induced polarization cross-talk. In particular, it significantly reduces cross-talk between circular and linear polarization, which limits the accuracy of today's solar single-beam polarimeters. We found that the technique works over a wide wavelength range in the visible. However, the slow modulation comes with an additional polarimetric efficiency loss which depends on the wavelength, as the retardance of a zero-order retarder is chromatic. Additionally, the efficiency usually differs for the linear and circular polarization states. This allows to chose the retarder specifically for a certain scientific goal, for example the maximization of the efficiency for the linear polarization where needed. As we demonstrated, in the cases of optimized efficiency for the linear polarization states, a non-corrected Stokes V can still be calculated and does not get obsolete.

We tested the the slow modulation technique with both fast modulators available at IRSOL and find that it works well independently of the modulator type. This brings two additional advantages. For the PEM, the rotation of the modulator (required to measure full Stokes) is obsolete, reducing potential beam wobble. For the FLCM, high frequency polarized fringes are significantly reduced, a major advantage compared to Fourier filtering in the post-processing for correction.

As a simple and low quality optical element, spurious polarimetric effects might be induced by the retarder. However, they remain synchronously with the modulation, like a polarization offset. With the "pseudo"-demodulation applied, most of these effects are removed. We also found that we can improve slowly modulated measurements further by using full turns of the retarder and combine them to compensate for additional systematic differences of the retarder film.

The two most important properties of the retarder which need to be characterized are its retardance and the position of its optical axis. The first may introduce uncertainty in the polarization amplitude, while the latter introduces cross-talk between the two linear polarization states. We found that with the retarder film at IRSOL the relative amplitude uncertainty in the linear polarization states can be on the order of 2-3%. This can be optimized by improving the amplitude accuracy, which was out of the scope of this work. Residual amplitude errors which cannot be corrected using the slow modulation are unpolarized stray light and an inaccurate dark correction. Regarding the cross-talk between the linear polarization states, we have shown that this cannot be corrected at the IRSOL observatory by using the slow modulation technique. However, the contribution by the slow modulator is minimized when carefully calibrating the position of the optical axis to at least $0.5°$.

Another relevant performance criterion is the reduction of spatial resolution when the slow modulation technique is used. On the one hand, this is the result of the optical quality of the retarder film, which is difficult to optimize given the large diameter needed to place the retarder on front of the IRSOL telescope. A quantitative analysis of the image quality reduction at IRSOL is difficult, because the seeing conditions do not allow for a robust systematic comparison of the image quality with and without the slow modulator. On the other hand, slow modulation cycles on the order of half a minute reduces the achievable spatio-temporal resolution of observations. At IRSOL, observations rarely require (or due to the seeing achieve) high spatial resolution. Instead, the scientific focus is on high polarimetric sensitivity with relatively long integration times. In consequence, the additional reduction of spatio-temporal resolution due to the slow modulation is acceptable.

The technique introduced at the IRSOL observatory is based on very general principles and therefore its application is not limited to a specific setup, although the implementation might differ due to technical constraints (i.e., if the aperture is significantly larger than 0.5 m). For example, we successfully tested the technique at the 1.5 m GREGOR telescope on Tenerife, Spain. Here we introduced the slow modulator in the converged beam close to the secondary focus, which is ahead of any oblique mirrors or other elements altering the Stokes vector. Additionally, this position allowed to reduce the required aperture size of the retarder, allowing for a much better optical quality. Applying this technique to a larger aperture telescope with a high optical quality retarder allows for testing the spatial resolution limits, opening the possibility to obtain challenging scattering polarization measurements with high spatial resolution.

Although so far the application of the method concentrates on spectrograph observations, in principle there is no limitation to such systems. For example, imaging spectropolarimetry using narrow band filters (e.g., based on Fabry-Pérot etalons) should also greatly benefit. This we plan to test in the future.

Acknowledgments

We thank David Harrington for useful comments and suggestions. This project has received funding from the European's Horizon 2020 research and innovation programme under grant agreement no 824135. IRSOL is supported by the Swiss Confederation (SEFRI), Canton Ticino, the city of Locarno and the local municipalities. This project has made use of *matplotlib*[41] and NASA ADS. Measuring solar polarization with high absolute accuracy was proposed and developed with support of the ERC Advance Grant project HotMol ERC-2011-AdG-291659.

REFERENCES

[1] F. A. Iglesias and A. Feller, "Instrumentation for solar spectropolarimetry: state of the art and prospects," *Optical Engineering* **58**(08), 082417 (2019).

[2] L. Bellot Rubio and D. Orozco Suárez, "Quiet Sun magnetic fields : an observational view," *Living Reviews in Solar Physics* **123** (2019).

[3] S. V. Berdyugina, A. V. Berdyugin, and V. Piirola, "Molecular Magnetic Dichroism in Spectra of White Dwarfs," *Physical Review Letters* **99**, 091101 (2007).

[4] A. V. Berdyugin, V. Piirola, S. Bagnulo, *et al.*, "Highly sensitive search for magnetic fields in white dwarfs using broad-band circular polarimetry," *Astronomy & Astrophysics* **657**, A105 (2022).

[5] J. O. Stenflo and C. U. Keller, "The second solar spectrum. A new window for diagnostics of the Sun.," *Astronomy & Astrophysics* **934**, 927–934 (1997).

[6] D. M. Fluri and J. O. Stenflo, "Continuum polarization in the solar spectrum," *Astronomy & Astrophysics* **341**, 902–911 (1999).

[7] J. O. Stenflo, "Polarization of the Sun's continuous spectrum," *Astronomy & Astrophysics* **429**, 713–730 (2005).

[8] A. Gandorfer, *The Second Solar Spectrum: A high spectral resolution polarimetric survey of scattering polarization at the solar limb in graphical representation. Volume II: 3910 Å to 4630 Å*, Zurich: VdF (2002).

[9] W. Hanle, "Über magnetische Beeinflussung der Polarisation der Resonanzfluoreszenz," *Zeitschrift für Physik* **30**, 93–105 (1924).

[10] J. O. Stenflo, C. U. Keller, and A. Gandorfer, "Differential Hanle effect and the spatial variation of turbulent magnetic fields on the Sun," *Astronomy & Astrophysics* **329**(1), 319–328 (1998).

[11] S. V. Berdyugina and D. M. Fluri, "Evidence for the Hanle effect in molecular lines," *Astronomy & Astrophysics* **417**, 775–784 (2004).

[12] J. Trujillo Bueno, N. Shchukina, and A. Asensio Ramos, "A substantial amount of hidden magnetic energy in the quiet Sun," *Nature* **430**(6997), 326–329 (2004).

[13] J. Trujillo Bueno, "Quantum spectropolarimetry and the Sun's hidden magnetism," in *Proceedings of the 11th European Solar Physics Meeting*, D. Danesy, S. Poedts, A. de Groof, *et al.*, Eds., *ESA Special Publication* **11**, 7.1 (2005).

[14] J. O. Stenflo, "Stokes polarimetry of the Zeeman and Hanle effects," *Observing Photons in Space* **21**, 66 (2013).

[15] A. Asensio Ramos and M. Collados, "Error propagation in polarimetric demodulation," *Applied Optics* **47**(14), 2541–2549 (2008).

[16] T. del Pino Alemán, J. Trujillo Bueno, J. Štěpán, *et al.*, "A Novel Investigation of the Small-Scale Magnetic Activity of the Quiet Sun Via the Hanle Effect in the Sr I 4607 Å Line," *The Astrophysical Journal* **863**(2), 20 (2018).

[17] A. G. de Wijn, R. Casini, A. Carlile, *et al.*, "The Visible Spectro-Polarimeter of the Daniel K . Inouye Solar," *Solar Physics* **297**, 22 (2022).

[18] S. V. Berdyugina, D. Gisler, F. Zeuner, *et al.*, "Scattering in an average quiet solar photosphere tested with absolute polarimetry in the optical continuum spectrum." (2022).

[19] F. Zeuner, L. Belluzzi, N. Guerreiro, *et al.*, "Hanle rotation signatures in Sr I 4607 Å," *Astronomy & Astrophysics* **662**, A46 (2022).

[20] K. Ichimoto, B. Lites, D. Elmore, *et al.*, "Polarization calibration of the solar optical telescope onboard hinode," *Solar Physics* **249**(2), 233–261 (2008).

[21] J. Tinbergen, "Accurate Optical Polarimetry with Nasmyth Telescopes," *Publications of the Astronomical Society of the Pacific* **119**(862), 1371–1384 (2007).

[22] V. Piirola, A. Berdyugin, and S. Berdyugina, "DIPOL-2: a double image high precision polarimeter," in *Ground-based and Airborne Instrumentation for Astronomy V*, S. K. Ramsay, I. S. McLean, and H. Takami, Eds., *Society of Photo-Optical Instrumentation Engineers (SPIE) Conference Series* **9147**, 91478I (2014).

[23] V. Piirola, I. A. Kosenkov, A. V. Berdyugin, *et al.*, "Double Image Polarimeter—Ultra Fast: Simultaneous Three-color (BV R) Polarimeter with Electron-multiplying Charge-coupled Devices," *The Astronomical Journal* **161**, 20 (2021).

[24] A. V. Berdyugin, S. V. Berdyugina, and V. Piirola, "High-precision and high-accuracy polarimetry of exoplanets," in *Ground-based and Airborne Instrumentation for Astronomy VII*, C. J. Evans, L. Simard, and H. Takami, Eds., *Society of Photo-Optical Instrumentation Engineers (SPIE) Conference Series* **10702**, 107024Z (2018).

[25] A. López Ariste, J. Rayrole, and M. Semel, "First results from THEMIS spectropolarimetric mode," *Astronomy and Astrophysics Supplement Series* **142**(1), 137–148 (2000).

[26] A. Skumanich, B. W. Lites, V. Martínez Pillet, *et al.*, "The Calibration of the Advanced Stokes Polarimeter," *The Astrophysical Journal Supplement Series* **110**(2), 357–380 (1997).

[27] A. Derks, C. Beck, and V. Martínez Pillet, "Inferring telescope polarization properties through spectral lines without linear polarization," *Astronomy & Astrophysics* **615**, A22 (2018).

[28] D. M. Harrington, S. Sueoka, A. J. White, *et al.*, "Polarization modeling and predictions for Daniel K. Inouye Solar Telescope, part 7: preliminary NCSP system calibration and model fitting," *Journal of Astronomical Telescopes, Instruments, and Systems* **7**(1), 1 – 57 (2021).

[29] R. Ramelli, D. Gisler, M. Bianda, *et al.*, "First successful deployment of the ZIMPOL-3 system at the GREGOR telescope," in *Ground-based and Airborne Instrumentation for Astronomy V*, S. K. Ramsay, I. S. McLean, and H. Takami, Eds., *Society of Photo-Optical Instrumentation Engineers (SPIE) Conference Series* **9147**, 91473G (2014).

[30] H. M. Schmid, A. Bazzon, R. Roelfsema, *et al.*, "SPHERE/ZIMPOL high resolution polarimetric imager," *Astronomy & Astrophysics* **619**, A9 (2018).

[31] A. M. Gandorfer, H. P. Povel, P. Steiner, *et al.*, "Solar polarimetry in the near uv with the zurich imaging polarimeter zimpol ii," *Astronomy & Astrophysics* **422**, 703–708 (2004).

[32] R. Ramelli, S. Balemi, M. Bianda, *et al.*, "ZIMPOL-3: a powerful solar polarimeter," in *Ground-based and Airborne Instrumentation for Astronomy III*, **7735**, 7735Y, SPIE Press (2010).

[33] B. W. Lites, "Rotating waveplates as polarization modulators for Stokes polarimetry of the sun: evaluation of seeing-induced crosstalk errors," *Applied Optics* **26**(18), 3838 (1987).

[34] J. C. del Toro Iniesta, *Introduction to Spectropolarimetry*, Cambridge University Press (2004).

[35] A. Feller, *Instrument Systems for Imageing Spectro-Polarimetry*. PhD thesis, ETH Zürich (2007).

[36] J. C. del Toro Iniesta and M. Collados, "Optimum modulation and demodulation matrices for solar polarimetry," *Applied Optics* **39**(10), 1637–1642 (2000).

[37] R. Ramelli, M. Bianda, L. Merenda, *et al.*, "The Hanle and Zeeman Effects in Solar Spicules," in *SOLAR POLARIZATION 4 ASP Conference Series*, R. Casini and B. W. Lites, Eds., **358**, 448, Astron. Soc. Pacific Conf. Ser (2006).

[38] J. Sánchez Almeida, V. Martínez Pillet, and A. D. Wittmann, "The instrumental polarization of a Gregory-Coude telescope," *Solar Physics* **134**, 1–13 (1991).

[39] D. M. Harrington, S. A. Jaeggli, T. A. Schad, *et al.*, "Polarization modeling and predictions for Daniel K. Inouye Solar Telescope, part 6: fringe mitigation with polycarbonate modulators and optical contact calibration retarders," *Journal of Astronomical Telescopes, Instruments, and Systems* **6**(03), 1 (2020).

[40] A. Gandorfer and H. P. Povel, "First observations with a new imaging polarimeter," *Astronomy & Astrophysics* **328**, 381–389 (1997).

[41] J. D. Hunter, "Matplotlib: A 2d graphics environment," *Computing in Science & Engineering* **9**(3), 90–95 (2007).

6. APPENDIX

6.1 Ideal linear retarder Mueller matrix and specific combinations

The ideal linear Mueller matrix for retarders with retardance $r = \frac{\delta}{2\pi}$ (phase shift δ in radians) and orientation θ of the optical axis is in general:

$$\mathbf{M}(\theta,\delta) = \begin{pmatrix} 1 & 0 & 0 & 0 \\ 0 & \cos^2 2\theta + \sin^2 2\theta \cos\delta & \cos 2\theta \sin 2\theta\,(1-\cos\delta) & \sin 2\theta \sin\delta \\ 0 & \cos 2\theta \sin 2\theta\,(1-\cos\delta) & \cos^2 2\theta \cos\delta + \sin^2 2\theta & -\cos 2\theta \sin\delta \\ 0 & -\sin 2\theta \sin\delta & \cos 2\theta \sin\delta & \cos\delta \end{pmatrix} \tag{17}$$

For $\theta_1 = 0°, \theta_2 = 45°, \theta_3 = 90°, \theta_4 = 135°$:

$$\mathbf{M}_1 = \mathbf{M}(\theta_1,\delta) = \begin{pmatrix} 1 & 0 & 0 & 0 \\ 0 & 1 & 0 & 0 \\ 0 & 0 & \cos\delta & -\sin\delta \\ 0 & 0 & \sin\delta & \cos\delta \end{pmatrix} \tag{18}$$

$$\mathbf{M}_2 = \mathbf{M}(\theta_2,\delta) = \begin{pmatrix} 1 & 0 & 0 & 0 \\ 0 & \cos\delta & 0 & \sin\delta \\ 0 & 0 & 1 & 0 \\ 0 & -\sin\delta & 0 & \cos\delta \end{pmatrix} \tag{19}$$

$$\mathbf{M}_3 = \mathbf{M}(\theta_3,\delta) = \begin{pmatrix} 1 & 0 & 0 & 0 \\ 0 & 1 & 0 & 0 \\ 0 & 0 & \cos\delta & \sin\delta \\ 0 & 0 & -\sin\delta & \cos\delta \end{pmatrix} \tag{20}$$

$$\mathbf{M}_4 = \mathbf{M}(\theta_4,\delta) = \begin{pmatrix} 1 & 0 & 0 & 0 \\ 0 & \cos\delta & 0 & -\sin\delta \\ 0 & 0 & 1 & 0 \\ 0 & \sin\delta & 0 & \cos\delta \end{pmatrix} \tag{21}$$

6.1.1 Linear polarization correction

First we will show that the currently applied method to correct Stokes Q and U is working independently of δ because $\mathbf{K}$ is diagonal.

$\mathbf{K}$ is given by combining the previous four matrices in a specific way:

$$\mathbf{K} = \mathbf{M}_1 - \mathbf{M}_2 + \mathbf{M}_3 - \mathbf{M}_4 = 2 \cdot (1 - \cos\delta) \begin{pmatrix} 0 & 0 & 0 & 0 \\ 0 & 1 & 0 & 0 \\ 0 & 0 & -1 & 0 \\ 0 & 0 & 0 & 0 \end{pmatrix} \tag{22}$$

Therefore, $\mathbf{K}$ is diagonal and $K_{22} = 2 \cdot (1 - \cos\delta) = -K_{33}$. Usually, δ is a function of the wavelength (there may be spatial inhomogeneities of the retardance for large apertures, too). Consequently, if $\delta(\lambda)$ is characterized for a given wavelength, K_{22} is known.

6.1.2 Circular polarization correction

Starting again from the four matrices, but now building a difference instead of a sum, results in $\mathbf{L}$, with $L_{24} = L_{34} = 2 \cdot \sin\delta$:

$$\mathbf{L} = \mathbf{M}_3 - \mathbf{M}_4 - (\mathbf{M}_1 - \mathbf{M}_2) = 2 \cdot \sin\delta \begin{pmatrix} 0 & 0 & 0 & 0 \\ 0 & 0 & 0 & 1 \\ 0 & 0 & 0 & 1 \\ 0 & -1 & -1 & 0 \end{pmatrix}. \tag{23}$$